Supporting Information to :

Small-angle scattering by supported nanoparticles: exact results and useful approximations

Cedric J. Gommes,* Tristan Asset, and Jakub Drnec

I. NITROGEN ADSORPTION-DESORPTION CHARACTERIZATION OF THE SUPPORT

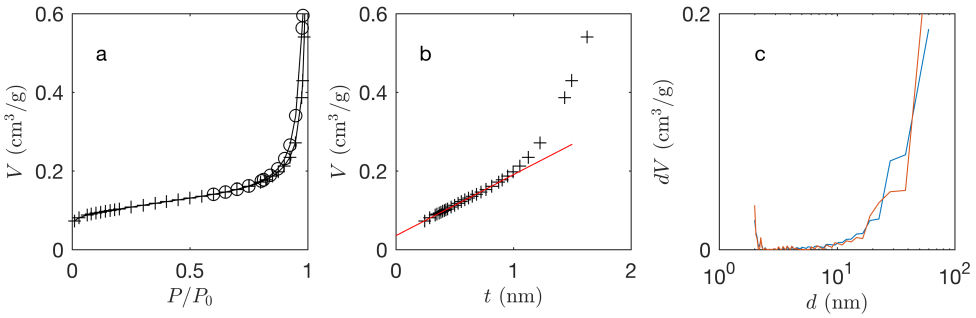

FIG. SI-1. Adsorption and desorption isotherms measured on the empty Vulcan support (a, + adsorption and ∘ desorption), t-plot obtained from the adsorption branch, with the least-square fit (red) from which the surface area (excluding micropores) the micropore volume are obtained (b), and mesopore size distribution obtained with the Derjaguin-Broekhoff-de Boer method (c, adsorption in red and desorption in blue).

The nitrogen adsorption/desorption isotherms measured on the Vulcan support is shown in Fig. SI-1a, from which one can make the following qualitative observations [1]. The fact that the isotherms do not reach a plateau close to saturation testifies to a mostly macroporous structure (*i.e.* with pores larger than 50 nm). The slight adsorption/desorption hysteresis suggests also at the presence of mesopores (with size between 2 and 50 nm). Moreover, the shape of the isotherms at small pressures hints at micropores (smaller than 2 nm).

Figure SI-1b displays a so-called t-plot, by which the quantity of nitrogen adsorbed at a given pressure is plotted against the statistical thickness t of the adsorbed layer at that particular pressure. The expression for the the pressure-dependent thickness t is the same as in [2]. The slope of the linear fit (see figure) provides the so-called external surface area $S_{ext} \simeq 140$ m^2/g, and the intercept provides the micropore volume $V_\mu \simeq 0.038$ cm^3/g. The surface area S_{ext} is *external* to the micropores; it accounts for both the meso and macropores.

Figure SI-1c plots the pore-size distribution obtained from the adsorption and desorption isotherms in Fig. SI-1a, using the Derjaguin-Brokehof-de Boer method [2]. Globally, the pore-size distribution confirms the qualitative assessment based on the shape of the isotherms, namely: the material comprises a few large mesopores and macropores (the distributions do not level-off for large pores).

The qualitative aspect of the structure are sketched in Fig. SI-2. Because the resolution of the SAXS is larger than the micropores, the micropore structure is accounted for in the main text by treating the carbon and micropores as an effective homogeneous medium with density lower than the carbon. The carbon density in the Vulcan support, measured by Helium pycnometry is $\bar{\rho}_C = 1.95$ g/cm^3 [3]. Based on that value, the effective density of the microporous

* cedric.gommes@uliege.be

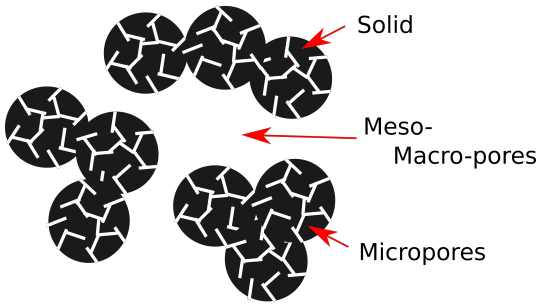

FIG. SI-2. Qualitative sketch of the Vulcan structure, comprising microporous carbon structures separated by pores in the meso- macropore size range.

carbon is calculated as

$$\bar{\rho}_S = \frac{\bar{\rho}_C}{1+1+\bar{\rho}_C V_\mu} \simeq 1.81 \text{ g/cm}^3 \tag{SI-1}$$

where we use the general notation $\bar{\rho}_X$ for the specific mass [g/cm^3] to distinguish it from the electron density ρ_X [F/cm^3].

II. DERIVATION OF EQS. (26) AND (29) OF THE MAIN TEXT

Using the same notations a in Sec. 4.2 of the main text, the indicator function of the metal nanoparticles is defined as

$$\mathcal{I}_P(\mathbf{x}) = \sum_i p_i\left(\mathbf{x}-\mathbf{x}_i\right) \tag{SI-2}$$

where $\mathcal{I}_P$ is the indicator function of the set of all particles, and p_i is the indicator function of the i^{th} particle specifically. The positions $\mathbf{x}_i$ are homogeneously distributed within a loading region L. The probability density distribution of the centre $\mathbf{x}$ of any particle is therefore $\mathcal{I}_L(\mathbf{x})/V_L$, where $\mathcal{I}_L$ is the indicator function of the loading region and V_L is its volume.

The volume fraction of the particles, ϕ_P, is calculated as the average value of $\mathcal{I}_P(\mathbf{x})$, *i.e.*

$$\phi_P = \frac{1}{V}\int \mathrm{d}V_x\ \mathcal{I}_P(\mathbf{x}) = \frac{N_p}{V}\langle V_p\rangle \tag{SI-3}$$

where N_p is the number of particles, and the integral is over $\mathbf{x}$ with the integration volume V is taken as infinitely large. The second equality results from

$$\langle V_p\rangle = \frac{1}{N_p}\sum_i \int \mathrm{d}V_x\ p_i(\mathbf{x}) \tag{SI-4}$$

One has to evaluate the limit of these expressions when the integration volume becomes infinitely large with $N_p/V_L = \theta_p$ kept constant, where V_L is the volume of the loading regions. One finds

$$\phi_P = \theta_p \phi_L \langle V_p\rangle \tag{SI-5}$$

where $\phi_L = V_L/V$ is the volume fraction of the loading region.

The covariogram of the particle phase is evaluated as

$$C_{PP}(\mathbf{r}) = \frac{1}{V}\sum_{ij}\int \mathrm{d}V_x\ p_i(\mathbf{x}-\mathbf{x}_i+\mathbf{r})p_j(\mathbf{x}-\mathbf{x}_j) \tag{SI-6}$$

with the same implicit limit here as above, namely that the integration volume becomes infinitely large, with the number of particles increasing like $N_p = \theta_p V_L$, with $V_L = \phi_L V$. Splitting the contributions $i=j$ from $i\neq j$ in the

sum leads to

$$C_{PP}(\mathbf{r}) = \frac{N_p}{V} K(\mathbf{r}) + \frac{1}{V} \sum_{i \neq j} \tilde{K}(\mathbf{x}_j - \mathbf{x}_i + \mathbf{r}) \tag{SI-7}$$

where the geometrical covariogram of the individual particles is defined as

$$K(\mathbf{r}) = \left\langle \int p_i(\mathbf{x}+\mathbf{r}) p_i(\mathbf{x}) \, \mathrm{d}V_x \right\rangle \tag{SI-8}$$

where the brackets mean here the average over all the parameters that define the shape and size of the i^{th} particle. The other covariogram-like quantity $\tilde{K}(r)$ is defined as

$$\tilde{K}(\mathbf{r}) = \left\langle \int p_i(\mathbf{x}+\mathbf{r}) p_j(\mathbf{x}) \, \mathrm{d}V_x \right\rangle = \int \langle p_i(\mathbf{x}+\mathbf{r}) \rangle \langle p_j(\mathbf{x}) \rangle \, \mathrm{d}V_x \tag{SI-9}$$

where $i \neq j$. The second equality results from assuming that the parameters that characterize the size and shape of two different particles i and j are statistically independent.

The first term in Eq. (SI-7) can be written as $\theta_p \phi_L K(\mathbf{r})$. The second sum in Eq. (SI-7) can be evaluated by writing the sum over $\mathbf{x}_i$ and $\mathbf{x}_j$ like integrals over the entire volume of the loading region L, *i.e.* replacing

$$\sum_{i \neq j} \to \theta_p^2 \int \mathrm{d}V_{x_i} \int \mathrm{d}V_{x_j} \, \mathcal{I}_L(\mathbf{x}_i) \mathcal{I}_L(\mathbf{x}_j) \tag{SI-10}$$

where $\mathcal{I}_L$ is the indicator function of the loading region. This is equivalent to assuming that the particles are uniformly distributed in the layer L. After a few algebraic manipulations, notably a change of variable $\delta = \mathbf{x}_i - \mathbf{x}_j$, one obtains

$$C_{PP}(\mathbf{r}) = \phi_L \theta_p K(\mathbf{r}) + \theta_p^2 \int \mathrm{d}V_\delta \, C_{LL}(\delta) \tilde{K}(\delta + \mathbf{r}) \tag{SI-11}$$

where the covariogram of the loading region appears as

$$C_{LL}(\delta) = \frac{1}{V} \int \mathrm{d}V_x \, \mathcal{I}_L(\mathbf{x}+\delta) \mathcal{I}_L(\mathbf{x}) \tag{SI-12}$$

The quantity that appears in the general expression for the $\bar{C}_\rho$ (Eq. 16 of the main text) is not strictly C_{PP}, but the centred covariogram $\bar{C}_{PP}$, which is obtained as

$$\bar{C}_{PP} = C_{PP} - \phi_P^2 \tag{SI-13}$$

From Eq. (SI-5), the quantity ϕ_P^2 can conveniently be written as

$$\phi_P^2 = \theta_p^2 \phi_L^2 \int \mathrm{d}V_x \tilde{K}(\mathbf{x}) \tag{SI-14}$$

because it results from the definition of $\tilde{K}$ that $\langle V_g \rangle^2$ is equal to the integral of $\tilde{K}$. The final expression we obtain for the centred covariogram is

$$\bar{C}_{PP}(\mathbf{r}) = \phi_L \theta_p K(\mathbf{r}) + \theta_p^2 \int \mathrm{d}V_\delta \, \bar{C}_{LL}(\delta) \tilde{K}(\delta + \mathbf{r}) \tag{SI-15}$$

where $\bar{C}_{LL}$ is the centred covariogram of the loading region.

Another quantity relevant to scattering is the cross-covariogram

$$C_{SP}(\mathbf{r}) = \frac{1}{V} \int \mathrm{d}V_x \, \mathcal{I}_S(\mathbf{x}) \mathcal{I}_P(\mathbf{x}+\mathbf{r}) = \frac{1}{V} \sum_i \int \mathrm{d}V_x \, \mathcal{I}_S(\mathbf{x}+\mathbf{r}) p_i(\mathbf{x}+\mathbf{r}-\mathbf{x}_i) \tag{SI-16}$$

Evaluating the sum as previously, that is replacing

$$\sum_i \to \theta_p \int_V \mathrm{d}V_{x_i} \, \mathcal{I}_L(\mathbf{x}_i) \tag{SI-17}$$

one finds

$$C_{SM}(\mathbf{r}) = \theta_p \int \mathrm{d}V_\delta \; C_{SL}(\delta)\langle p(\mathbf{r}+\delta)\rangle \tag{SI-18}$$

where $\langle p()\rangle$ is the average value of the particle profile $p()$, and

$$C_{SL}(\delta) = \frac{1}{V}\int \mathrm{d}V_x \; \mathcal{I}_S(\mathbf{x}+\delta)\mathcal{I}_L(\mathbf{x}) \tag{SI-19}$$

is the cross-covariogram of phases S and L. The centred cross-covariogram is eventually obtained as

$$\bar{C}_{SP}(\mathbf{r}) = \theta_p \int \mathrm{d}V_\delta \; \bar{C}_{SL}(\delta)\langle p(\mathbf{r}+\delta)\rangle \tag{SI-20}$$

which is the expression needed to evaluate the scattered intensity.

III. ASYMPTOTIC EXPRESSIONS OF THE COVARIANCES $C_{SS}(r)$, $C_{LL}(r)$ AND $C_{SL}(r)$ IN FIG. 4

A. Solid-solid covariance $C_{SS}(r)$

The covariance $C_{SS}(r)$ is the probability that two points at distance r from one another both belong to the solid phase of the porous material. Let the two points be called A and B. In the approximation of Fig. 4 of the main text (flat surface and infinite solid), the covariance can be decomposed as

$$C_{SS}(r) = \int_0^\infty a_S \mathrm{d}z \quad \mathrm{P}\left(B \in S | A \text{ at depth } \; z\right) \tag{SI-21}$$

where $a_S\mathrm{d}z$ is the probability for a randomly chosen point to be in the solid at distance z from the surface, and $\mathrm{P}\left(B \in S | A \text{ at depth } \; z\right)$ is the conditional probability for point B to be in the solid, given that point A is at depth z. The latter conditional probability is

$$\mathrm{P}\left(B \in S | A \text{ at depth } \; z\right) = \begin{cases} (r+z)/(2r) & \text{for} \quad z < r \\ 1 & \text{for} \quad z \geq r \end{cases} \tag{SI-22}$$

The case for $z < r$ results from evaluating the fraction of the sphere with radius r and centre at depth z that is in the solid.

The result can be written formally as

$$\begin{aligned} C_{SS}(r) &= \int_0^\infty a_S \mathrm{d}z + \frac{a_S}{2r}\int_0^r \mathrm{d}z \; (z-r) \\ &= \phi_S - \frac{a_S}{4} r \end{aligned} \tag{SI-23}$$

where the second equality results from equating $\int_0^\infty a_S \mathrm{d}z = \phi_S$.

B. Covariance $C_{SL}(r)$ between the solid and the layer

The decomposition is the same as for C_{SS}, namely

$$C_{SL}(r) = \int_0^\infty a_S \mathrm{d}z \quad \mathrm{P}\left(B \in L | A \text{ at depth } \; z\right) \tag{SI-24}$$

We use the notation $g = d - t/2$ for the gap between the solid and the layer (see Fig. 4 of the main text).

If $r < g$, there is no way for two points at distance r from one another to be in S and in L, respectively. The probability is therefore

$$\mathrm{P}\left(B \in L | A \text{ at depth } \; z\right) = 0 \tag{SI-25}$$

and $C_{SL}(r) = 0$ for $r < g$.

If $g \leq r < g+t$, two cases are to be considered, depending on the position z of point A, namely

$$\mathrm{P}\left(B \in L | A \text{ at depth } z\right) = \begin{cases} (r-g-z)/(2r) & \text{for} \quad z < r-g \\ 0 & \text{for} \quad z \geq r-g \end{cases} \tag{SI-26}$$

The case for $z < r-g$ results from considering a sphere with radius r and centre at depth z in the solid, and evaluating the fraction of its surface that intersects the layer. As a consequence

$$C_{SL}(r) = \int_0^{r-g} a_S \mathrm{d}z \quad \frac{r-g-z}{2r} = \frac{a_S}{4r}(r-g)^2 \tag{SI-27}$$

If $r > g+t$, three cases have to be considered

$$\mathrm{P}\left(B \in L | A \text{ at depth } z\right) = \begin{cases} t/(2r) & \text{for} \quad z < r-g-t \\ (r-g-z)/(2r) & \text{for} \quad r-g-t \leq r < r-g \\ 0 & \text{for} \quad r-g \leq z \end{cases} \tag{SI-28}$$

These values too result from considering a sphere with radius r and centre at depth z in the solid, and evaluating the fraction of its surface that intersects the layer. In the first case, the top of sphere is above the top of the layer; in the second case, the top of the sphere is inside the layer; in the last case, the top of the sphere does not touch the layer. As a consequence

$$\begin{aligned} C_{SL}(r) &= \int_0^{r-g-t} a_S \mathrm{d}z \quad \frac{t}{2r} + \int_{r-g-t}^{r-g} a_S \mathrm{d}z \quad \frac{r-g-z}{2r} \\ &= \frac{a_S}{4}\frac{t}{r}(r-d) \end{aligned} \tag{SI-29}$$

C. Layer-layer covariance $C_{LL}(r)$

To calculate C_{LL} we consider point A to be in L (as opposed to in S for C_{SS} and C_{SL}), and z is therefore the distance to the surface of the layer.

If $r < t/2$, the conditional probability is

$$\mathrm{P}\left(B \in L | A \text{ at depth } z\right) = \begin{cases} (r+z)/(2r) & \text{for} \quad z < r \\ 1 & \text{for} \quad z \geq r \end{cases} \tag{SI-30}$$

In consequence

$$\frac{1}{2}C_{LL}(r) = \int_0^{r} a_S \mathrm{d}z \quad \frac{r+z}{2r} + \int_r^{t/2} a_S \mathrm{d}z \tag{SI-31}$$

where the factor $1/2$ results from the symmetry of the layer, and it accounts for the fact that the integral on z is carried only on half of its thickness. The result for $r \leq t/2$ is eventually

$$C_{LL}(r) = \phi_L - \frac{a_S}{2}r \tag{SI-32}$$

where have have written $\phi_L = a_S t$.

For $t/2 \leq r < t$, the conditional probability is

$$\mathrm{P}\left(B \in L | A \text{ at depth } z\right) = \begin{cases} (r+z)/(2r) & \text{for} \quad z < t-r \\ t/(2r) & \text{for} \quad z \geq t-r \end{cases} \tag{SI-33}$$

The result for $t/2 < r \leq t$ happens to be the same as for $r \leq t/2$, namely

$$C_{LL}(r) = \phi_L - \frac{a_S}{2}r \tag{SI-34}$$

For $t \leq r$, the conditional probability is

$$\mathrm{P}\left(B \in L | A \text{ at depth } z\right) = t/(2r) \tag{SI-35}$$

So that the covariance is simply

$$C_{LL}(r) = \phi_L \frac{t}{2r} \tag{SI-36}$$

which has the typical $1/r$ behaviour of surface correlation functions.

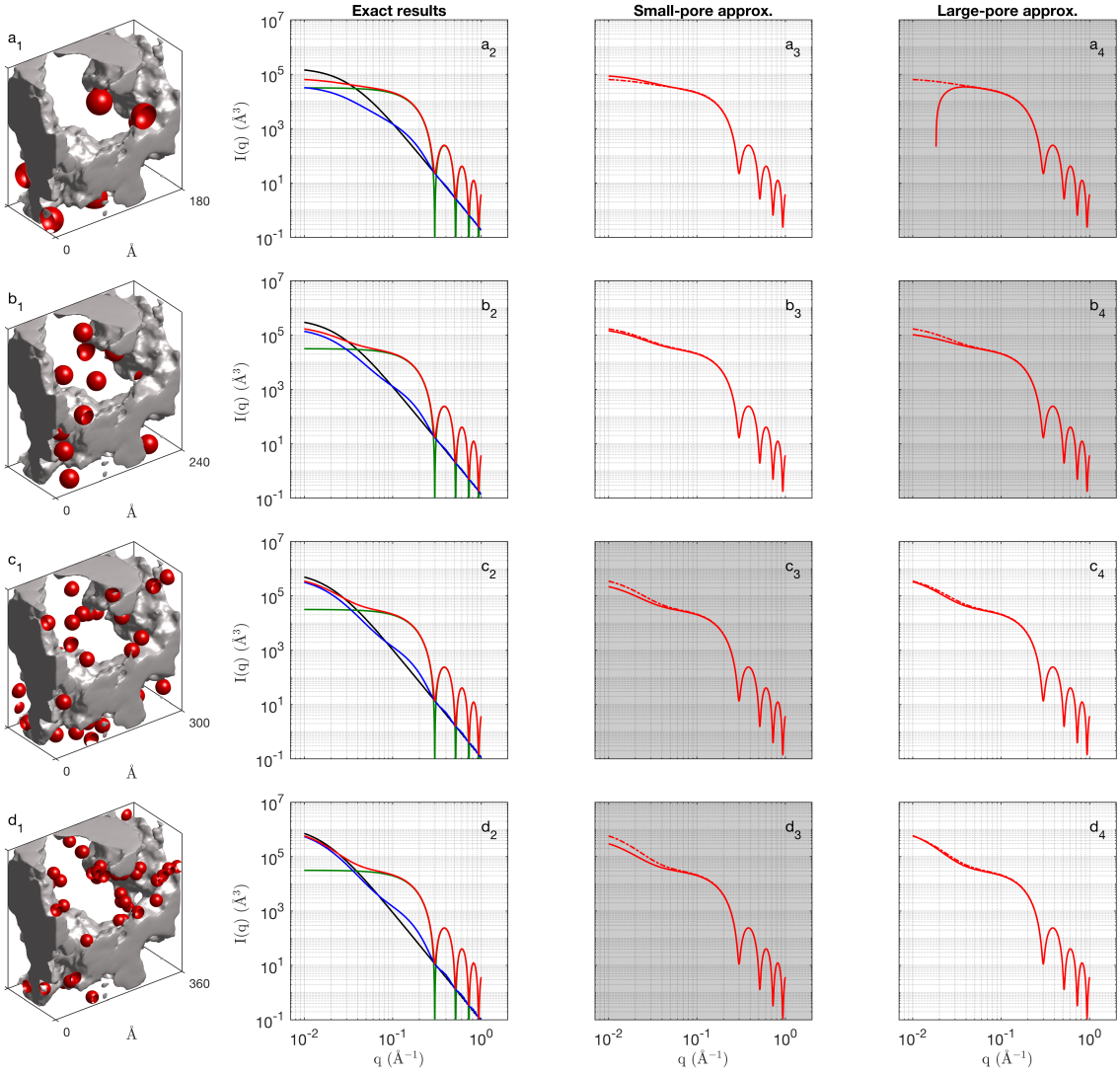

FIG. SI-3. Realizations (a_1 to d_1) and calculated SAXS patterns (a_2 to d_2) of GRF model of supported nanoparticles for increasingly large pores. The particle diameter is set to 30 Å and the pore chord length increases from $l_P = 3 \times 30$ Å (a), $l_P = 4 \times 30$ Å (b), $l_P = 5 \times 30$ Å (c) and $l_P = 6 \times 30$ Å (d). The various contributions of the SAXS patterns are the empty support (black), the particles (green), the support contribution deformed by contrast matching effects (blue), and total scattering (red). Figures a_3 to d_3, and a_4 and d_4, show the patterns calculated in the small-pore and large-pore approximations, respectively (solid red line). The dotted red line is the corresponding exact patterns (i.e. same as in a_2 to d_2). The grey shade highlight the cases where the approximations does not hold.

[1] S. J. Gregg and K. S. W. Sing, *Adsorption, Surface Area and Porosity* (Academic Press, London, 1982).
[2] C. J. Gommes, Langmuir **28**, 5101 (2012).
[3] S. Pérez-Rodrguez, D. Torres, and M. J. Lázaro, Powder Technology **340**, 380 (2018).